Volume 6 | Number 20 | 28 May 2018 | Pages 5303–5564

Journal of Materials Chemistry C

Materials for optical, magnetic and electronic devices

rsc.li/materials-c

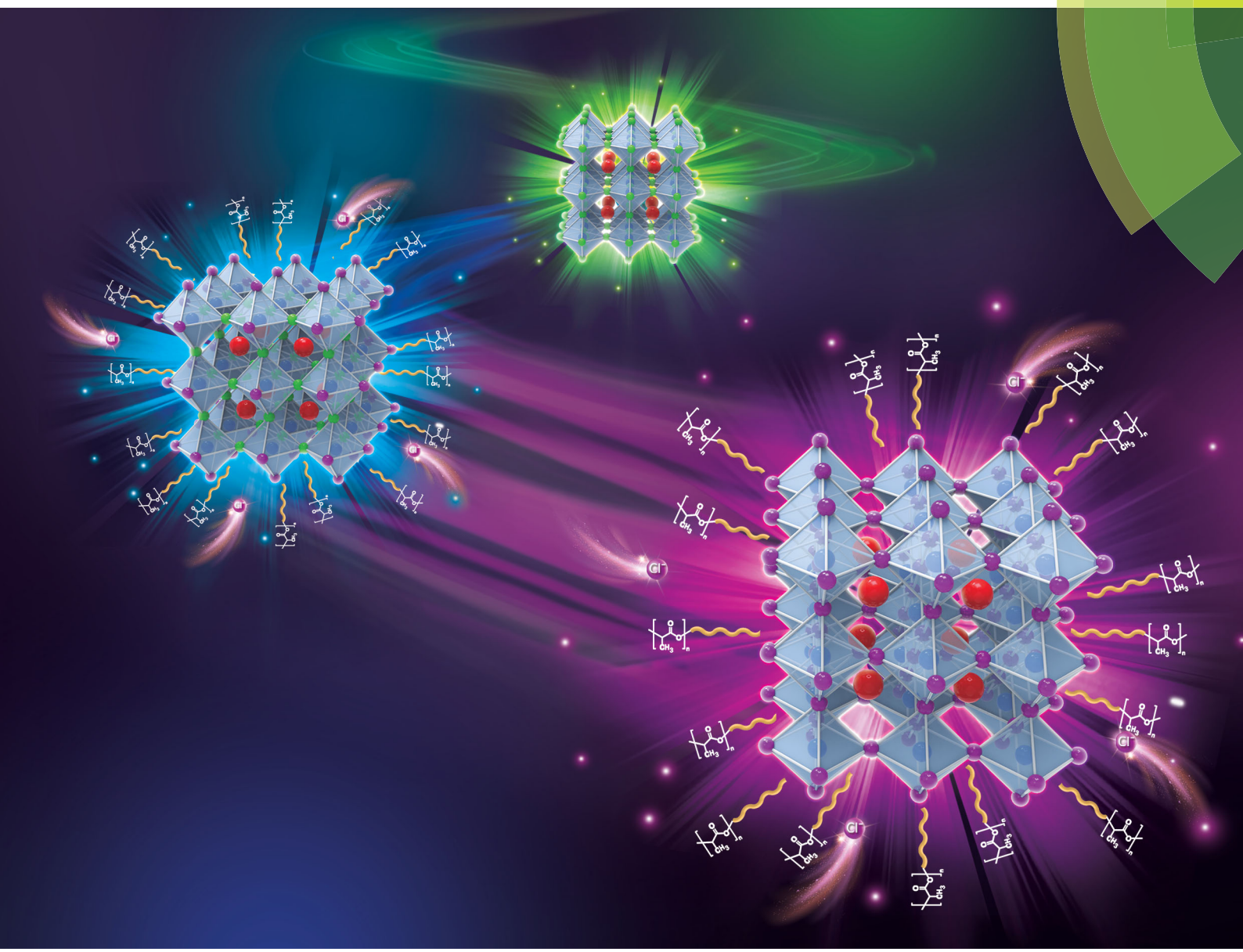

ISSN 2050-7526

ROYAL SOCIETY OF CHEMISTRY

PAPER

Zongtao Li, Jin Z. Zhang *et al.*

Tuning the emission spectrum of highly stable cesium lead halide perovskite nanocrystals through poly(lactic acid)-assisted anion-exchange reactions

Journal of Materials Chemistry C

PAPER

Check for updates

Cite this: J. Mater. Chem. C, 2018, 6, 5375

Tuning the emission spectrum of highly stable cesium lead halide perovskite nanocrystals through poly(lactic acid)-assisted anion-exchange reactions†

Longshi Rao,[ab] Yong Tang,[a] Caiman Yan,[a] Jiasheng Li,[a] Guisheng Zhong,[a] Kairui Tang,[c] Binhai Yu,[a] Zongtao Li *[a] and Jin Z. Zhang *[b]

Received 2nd February 2018, Accepted 16th April 2018

DOI: 10.1039/c8tc00582f

rsc.li/materials-c

We demonstrate an organic macromolecule-assisted anion-exchange reaction method for tuning the emission spectrum of cesium lead halide perovskite ($CsPbX_3$) nanocrystals (NCs) from green to near-ultraviolet using a microreactor. Using poly(lactic acid) (PLA), the emission peak of $CsPbX_3$ NCs can be tuned from 514 nm to 420 nm while maintaining high photoluminescence (PL) quantum yields (QYs) of 33–90%. By taking advantage of the microreactor, we synthesize parent $CsPbBr_3$ NCs and complete anion-exchange reactions at the same time, which is more efficient than most previously reported methods. The stability of $CsPbX_3$ NCs is improved by PLA coating, especially for $CsPbCl_3$, which shows long-term stability under ambient conditions for at least two weeks. The $CsPbBr_3$ NCs are utilized with a red phosphor on a blue light emitting-diode (LED) chip, achieving white light emission with a luminous efficacy of 62.93 lm W^{-1} under a 20 mA driving current. Highly efficient white LEDs (wLEDs) demonstrate the potential of halide perovskite NCs for optoelectronic applications, including low-cost displays, lighting, and optical communication.

1. Introduction

In recent years, cesium lead halide perovskite ($CsPbX_3$) nanocrystals (NCs) have received growing interest as a result of their novel properties, such as high charge carrier mobility, small exciton binding energy, large absorption coefficients and long exciton diffusion lengths.[1–5] Colloidal $CsPbX_3$ NCs have exhibited a high photoluminescence (PL) quantum yield (QY) of greater than 90% and a narrow emission bandwidth that can be easily tuned over the entire visible spectral region by controlling the crystal size and halide ion composition.[6–9] Furthermore, $CsPbX_3$ NCs with a narrow size distribution, high stability and short radiative lifetimes have been developed for green emission.[10–12] The outstanding properties of $CsPbX_3$ NCs distinguish them from traditional semiconductor materials and make them promising candidates for applications in light-emitting diodes,[13] solar cells,[14] field-effect transistors,[15] lasers,[16] and photodetectors.[17] Currently, the ability to precisely regulate the emission spectrum and improve stability for $CsPbX_3$ NCs is potentially useful for optoelectronic applications, including displays, lighting, and optical communication.[13,18,19] Therefore, there is growing interest in developing fast and simple methods for synthesizing $CsPbX_3$ NCs with tunable spectrum and high stability for practical applications.

Recently, postsynthetic ion-exchange reactions have attracted great attention in synthesizing $CsPbX_3$ NCs because they allow for fine control of the NCs and enable synthesis of previously inaccessible materials.[20–22] For example, Li *et al.*[22] reported novel disk-shaped hexagonal Cu_2Te NCs by ion-exchange from CdTe nanodisks, maintaining an uninterrupted ionic sublattice and preserving the pre-existing shape. Ion-exchange reactions have also been demonstrated for producing $CsPbX_3$ NCs with high PL QYs as well as narrow and tunable PL emission.[23–26] Previous studies have used both organic and inorganic halide precursors, such as Grignard reagents (MeMgX), oleylammonium halides (OAmX), PbX_2, LiX, ZnX_2 and tetrabutylammonium halides (X = Cl, Br, and I), for the anion-exchange reactions.[9,24,27–32] Ramasamy *et al.*[9] described a simple halide anion-exchange reaction method in $CsPbX_3$ NCs, where by adjusting the halide ion (LiX) concentration, the PL emission of these NCs can be tuned

[a] Engineering Research Centre of Green Manufacturing for Energy-Saving and New-Energy Technology, School of Mechanical and Automotive Engineering, South China University of Technology, Guangzhou, 510640, China. E-mail: meztli@scut.edu.cn

[b] Department of Chemistry and Biochemistry, University of California, Santa Cruz, CA 95064, USA. E-mail: zhang@ucsc.edu

[c] The Mechanical Engineering, Pennsylvania State University, Harrisburg, PA 17057, USA

† Electronic supplementary information (ESI) available. See DOI: 10.1039/c8tc00582f

from 425 to 655 nm. Nedelcu *et al.*[24] reported a feasible method for the synthesis of $CsPbX_3$ NCs with monodisperse colloidal nanocubes by anion-exchange reactions, where the halide sources included organometallic Grignard reagents (MeMgX), oleylammonium halides (OAmX) and PbX_2. Zhang *et al.*[31] demonstrated a facile approach to modulate the anion composition of $CsPbX_3$ NCs by employing ZnX_2 as the halide source. However, these methods usually need multiple steps to synthesize parent $CsPbBr_3$ NCs and complete the anion-exchange reactions, which result in poor stability, especially for near UV and red emitting $CsPbX_3$ NCs. In addition, both the time needed for completing the ion-exchange and the quality of the exchanged $CsPbX_3$ NCs are varied, depending on the type of halide sources. Besides, the anion-exchange reactions when the inorganic salts are halide sources are very intense and rapid during the recrystallization process, and it is hard to control the process and tune the properties of $CsPbX_3$ NCs.

Microreactors have increasingly drawn our attention because of their advantages, including their high speed mixing, controllable flow rates and high reproducibility.[33,34] In addition, microreactors can provide better choices than conventional reactors for the synthesis of products that require anaerobic anhydrous environments to avoid the degradation of certain sensitive compounds. These remarkable properties have allowed their broad applications in nanoparticle synthesis and medicine production.[35,36] However, there have been few reports on the synthesis of $CsPbX_3$ NCs using microreactors.[37–39] With this in mind, we devote ourselves to developing a microreactor for the highly efficient synthesis of $CsPbX_3$ NCs with high QY and tunable spectrum.

Among various previous reports on the anion-exchange reactions of $CsPbX_3$, several inorganic salts, such as LiX, ZnX_2, PbX_2 and CuX_2, were used as the halide source. To date, there are few reports on the effect of organic molecules on anion-exchange. Chen *et al.*[5] applied 2-phenoxyethylamine (POEA) into $CH_3NH_3PbBr_3$ solution to modulate the organic–inorganic hybrid perovskite structure from bulk to layered, and with a PL and electroluminescence (EL) shift from green to blue. Such an approach may be used for the PL spectral shift of $CsPbX_3$ NCs. In this work, we report an organic macromolecule-assisted anion-exchange reaction method for tuning the emission spectrum of highly stable $CsPbX_3$ NCs with a microreactor. X-ray diffraction (XRD), transmission electron microscopy (TEM) and energy-dispersive X-ray spectrometry (EDX) were performed to characterize the crystal structure and surface morphology of $CsPbX_3$ NCs. In addition, by optimizing the mass fractions of PLA and the volume ratio of PLA solution to parent $CsPbBr_3$ NC solution, the PL emission of $CsPbX_3$ NCs ranged from green to near-UV. Meanwhile, by taking advantage of the microreactor, we can synthesize colloidal solutions of parent $CsPbBr_3$ NCs and complete the anion-exchange reactions at the same time. The mechanism of interaction between PLA and colloidal $CsPbBr_3$ NCs was also investigated using experimental and theoretical verification. Finally, to evaluate the performance of the as-synthesized halide perovskite NCs for light emission applications, the $CsPbBr_3$ NCs are used with a red phosphor on a blue light-emitting diode (LED) chip, achieving a luminous efficacy of 62.93 lm W^{-1} for white light emission under a 20 mA driving current. This demonstrated the promise of halide perovskite NCs for potential applications, such as low-cost displays, lighting, and optical communication.

2. Experimental

2.1 Materials and chemicals

Cesium bromide (CsBr, 99.9%), lead bromide ($PbBr_2$, 99.9%), oleic acid (OA, 90%), oleylamine (OAm, 70%), dimethylformamide (DMF, 99.9%), *n*-hexane (99%), and 1,4-dioxane (99.7%) were purchased from Shanghai Aladdin Biochemical Technology Co. Toluene (anhydrous, 99.8%), chloroform (anhydrous, 99.8%), poly(lactic acid) (PLA, M_w 60 000), and poly(methyl methacrylate) (PMMA, M_w 50 000) were purchased from Sigma-Aldrich Co. Transparent silicone resin (OE-6650A and B) was purchased from Dow Corning Co., and the red phosphor $(Ba, Ca, Sr)_3SiO_5$:Eu was purchased from Nichia Co. The chemicals used in the present work were of analytical grade and used without further purifications.

2.2 Preparation of Cs-precursor, Pb-precursor and PLA solution

To prepare the Cs-precursor, CsBr (0.40 mmol) was dissolved in DMF (5.0 mL) under vigorous stirring and then OA (0.50 mL) and OAm (0.25 mL) were added to stabilize the precursor solution.

The preparation process of the Pb-precursor was similar to the Cs-precursor, and $PbBr_2$ (0.40 mmol), OA (0.50 mL), and OAm (0.25 mL) were added to DMF (5.0 mL) with vigorous stirring.

The PLA solution with a mass fraction ranging from 5% to 30% was dissolved in chloroform at room temperature with vigorous stirring until it was completely dissolved. Before use, the PLA solution was stirred at low speed to prevent solidification.

2.3 Anion-exchange reactions

A schematic diagram of anion-exchange reactions using a microreactor is shown in Fig. 1a. For the microreactor, the most important region is the microchannel with different channel shapes (Fig. 1b), which allows homogeneous mixing of precursors and completing the anion-exchange reactions. Before the precursors were injected, the microreactor system was purged with argon gas to remove any air and heated to remove any water. To synthesize parent $CsPbBr_3$ NCs, 2.0 mL of the Cs-precursor, 2.0 mL of the Pb-precursor and 20 mL of toluene were injected into the microreactor by syringe pump 1 at a certain rate (Cs-precursor, toluene and Pb-precursor were injected into 1, 2 and 3 inlets of the microchannel, respectively) at the same time. When the freshly prepared parent colloidal $CsPbBr_3$ NCs arrived ahead of outlet 4, PLA solution was injected by syringe pump 2 to join in anion-exchange reactions. The volume ratio of the PLA solution to parent $CsPbBr_3$ NCs solution was between 1 : 30 and 1 : 1 to ensure the generation of NCs with an emission peak ranging from the green to near UV

 This journal is © The Royal Society of Chemistry 2018

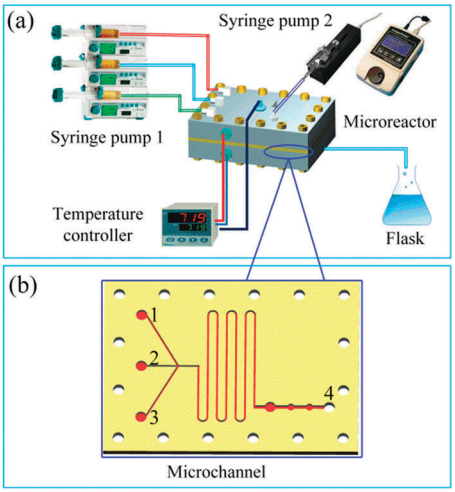

Fig. 1 (a) The schematic diagram of anion-exchange reactions using a microreactor. The microreactor system mainly consists of syringe pumps, a temperature controller, a microreactor, and a flask. (b) High-resolution image of the microchannel. The numbers 1, 2, and 3 represent three different inlets of the microchannel and 4 represents the outlet of the microchannel, respectively.

region. The products were collected by a round-bottom flask and stored in a drying cabinet.

In order to determine the stability of $CsPbCl_3$ NCs after the anion-exchange reactions were completed, we compared our method with a conventional inorganic anion-exchange method reported by Ramasamy *et al.*[9] With the conventional method, the parent $CsPbBr_3$ NC solution was synthesized following the procedure reported by Protesescu *et al.*,[40] and the anion-exchange reaction was carried out at room temperature by adding 20 μL of 0.64 M LiCl to 1.0 mL of $CsPbBr_3$ NCs *n*-hexane solution. Then, the mixture was shaken vigorously, observing a color change from green to colorless when the $CsPbCl_3$ NCs were obtained.

2.4 Preparation of halide perovskite white light-emitting diode (wLED) devices

The wLED devices mainly consist of a $CsPbBr_3$ NC film, a red phosphor film and a commercial blue LED chip. To fabricate a green $CsPbBr_3$ NC film, the as-synthesized $CsPbBr_3$ NCs were dispersed into a PMMA/chloroform solution and the mixture was vigorously stirred with a vacuum homogenizer for 6 min to degas bubbles. After that, the mixture was injected into a mold and heated at 60 °C for 2 h to remove the chloroform. The red phosphor film was prepared by adding red phosphors $(Ba, Ca, Sr)_3SiO_5$:Eu into the silicon gel (OE-6650A and B) and vigorously stirred with a vacuum homogenizer for 12 min to degas bubbles. Then, the mixture was injected into a mold and solidified in a vacuum oven at 80 °C for 30 min and at 150 °C for 2 h sequentially. Finally, the green and red film layers were coated on the surface of a blue LED chip (centred at 460 nm).

2.5 Measurement and characterization

The ultraviolet-visible (UV-vis) absorption spectra of $CsPbX_3$ NCs were measured using a UV-vis spectrometer (Shimadzu, Japan) over the wavelength range from 300 nm to 700 nm, at 1 nm interval. The PL spectra of the $CsPbX_3$ NCs were recorded on a fluorescence spectrophotometer (RF-6000, Shimadzu, Japan) using a Xe lamp as the excitation source. The phase purity and structure of the as-prepared NCs were measured using an X-ray diffractometer (XRD, D8-Advance, Bruker, Germany) with a Cu-Kα radiation source (λ = 0.15418 nm) at a counting rate of 2° per minute in the scanning angle (2θ) range from 5° to 50°. The crystal structure and surface morphology of the $CsPbX_3$ NCs were characterized by transmission electron microscopy (TEM, JEM-2100F, JEOL, Japan) at an accelerating voltage of 200 kV. The PL QY of the $CsPbX_3$ NCs was calculated using the following equation.[41,42]

$$Q = Q_{st}\frac{K_x}{K_{st}}\cdot\frac{\eta_x}{\eta_{st}} \quad (1)$$

where Q is the QY and the subscripts x and st denote the test and the standard, respectively. Quinine sulfate (the QY is 0.546 under 366 nm excitation) was used as the standard for blue and green spectral regions. K represents the slope determined by the ratio of the linear curves of the integrated fluorescence intensity to UV-vis absorption. η is the refractive index of the solvent. The integrated emission intensity is the area under the PL curve in the wavelength range of 380–600 nm.

3. Results and discussion

3.1 The crystal structure and morphology of $CsPbX_3$ NCs

The crystal structure and morphology of anion-exchanged $CsPbX_3$ NCs were characterized *via* XRD and TEM. Fig. 2 shows the XRD patterns of the $CsPbX_3$ NCs before and after the anion-exchange reactions. The diffraction patterns for the $CsPbX_3$ NCs have six broad peaks, corresponding to the (100), (110), (200), (102), (112), and (202) planes of the perovskite bulk counterparts (JCPDS No. 18-0364 and 18-0366), respectively.[43,44] In addition, the main diffraction peaks of the products gradually moved from $CsPbBr_3$ to $CsPbCl_3$ after PLA was added. These results indicated that the anion-exchange reactions were successfully completed and the basic framework of $CsPbX_3$ NCs was not broken, *i.e.*, the metal cations maintained their positions, and only the halide anions were replaced.

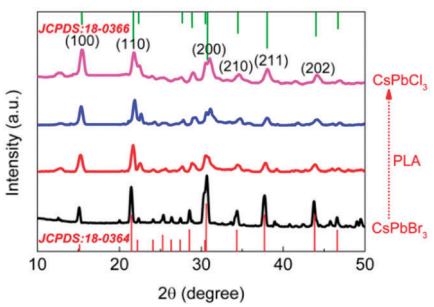

Fig. 2 XRD patterns of the $CsPbX_3$ NCs before and after anion-exchanged reactions. The black, red, blue, and pink lines represent the $CsPbBr_3$ NCs after treatment with PLA at different periods of time: 0 min, 30 min, 60 min, and 120 min, respectively.

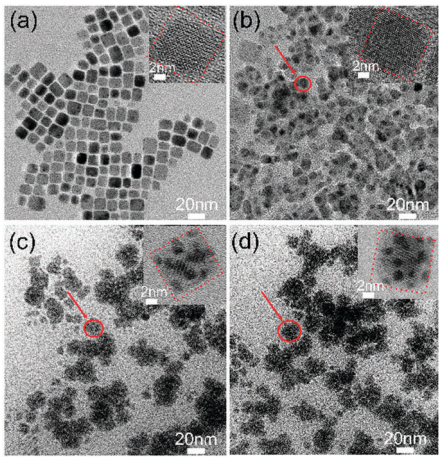

Fig. 3 TEM images of the $CsPbBr_3$ NCs after treatment with PLA at different periods of time: (a) 0 min, (b) 30 min, (c) 60 min, and (d) 120 min. Insets are high-resolution TEM (HRTEM) images, and red arrows with circle and red quadrilateral represent the crystal lattice testing area and single $CsPbX_3$ NC, respectively.

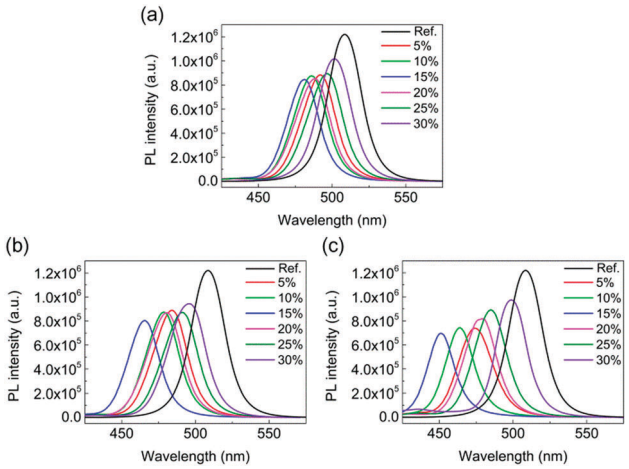

Fig. 4 The effect of PLA with different mass fractions on the $CsPbX_3$ PL spectral shift at different periods of time: (a) 30 min, (b) 60 min, and (c) 90 min.

The structure and morphology of parent $CsPbBr_3$ NCs and the as-prepared products were characterized using TEM, as shown in Fig. 3a–d. Without adding PLA, the parent $CsPbBr_3$ NCs are well dispersed and with an obvious crystal lattice, as shown in Fig. 3a. The high-resolution TEM (HRTEM) image of the parent $CsPbBr_3$ NCs provided in the inset shows the NCs with a clear lattice spacing distance of 0.58 nm. With the addition of PLA, the surface morphology of the $CsPbX_3$ NCs becomes amorphous because of PLA coating the surface of the NCs, while the crystal lattice of the NCs is still clear, as shown in Fig. 3b–d. Thus, it is obvious to identify that the crystal structure of the products has not been destroyed. Besides, the elemental composition of the products was measured by using EDX, as shown in Fig. S1 (ESI†), and the results revealed that the Br^- ion was successfully replaced by the Cl^- ion by adding PLA. Therefore, the XRD, TEM, and EDX results confirmed that the existence of anion-exchanged halide perovskite NCs.

3.2 Optimization of synthetic conditions and characterization of the optical properties of as-prepared $CsPbX_3$ NCs

To optimize the optical properties of the as-prepared $CsPbX_3$ NCs, the effect of PLA with 5–30% mass fractions on the PL spectral shift was investigated, as shown in Fig. 4a–c. The PLA solution was added to the $CsPbBr_3$ NCs and then the mixture was placed upon exposure to a 365 nm UV lamp in order to observe its color change *in situ.* The reference sample has no PLA added. 30 minutes after the addition of PLA, the PL spectra shown in Fig. 4a blue shifted 18 nm, 24 nm, 29 nm, 21 nm, 13 nm, and 9 nm corresponding to 5%, 10%, 15%, 20%, 25%, and 30% mass fractions of PLA, respectively. With longer times, the blue-shift of the PL spectra of the samples with PLA became more obvious, as shown in Fig. 4b and c. When the anion-exchange reactions were finished, the PL spectra blue-shifted 35 nm, 46 nm, 59 nm, 32 nm, 24 nm, and 19 nm corresponding to 5%, 10%, 15%, 20%, 25%, and 30% mass fractions of PLA, respectively. When the PLA mass fraction was $<15\%$, the larger PLA mass fraction results in a larger PL spectral blue-shift. However, when the mass fraction of PLA was $>15\%$, the PLA fraction has less impact on the PL spectral shift. This was especially true for a mass fraction of 30%, and the spectrum has a negligible shift. A lower mass fraction ($<15\%$) led to the Br^- and Cl^- anion-exchange reactions incompletely, while a higher mass fraction ($>15\%$) blocked the substitution of Cl^- for Br^- due to easy aggregation of PLA. Therefore, a suitable mass fraction can improve the interaction between the Br^- and Cl^-. However, the 30% fraction of PLA improves the $CsPbBr_3$ NC stability as the high concentration PLA can rapidly solidify. Taking all into consideration, the PLA with 15% mass fractions has the best effect on the $CsPbBr_3$ NCs PL spectral shift. Since the mass fractions of 15% resulted in the stronger spectral shift, in the following experiments, the PLA content of 15% was used.

In addition, we investigated the effect of the volume ratio of PLA solution to parent $CsPbBr_3$ NCs solution on the PL spectral shift and the time it takes for completing the anion-exchange reactions. Fig. S2 (ESI†) shows the effect of the volume ratio of PLA to parent $CsPbBr_3$ NCs on the PL spectral shift. The results reveal that the PL spectrum has the largest blue-shift when the volume ratio is 1 : 10. However, when the volume ratio is $<1:10$, the PLA has little effect on Br^- to Cl^- anion-exchange and the reaction took longer to complete (Fig. S2b, ESI†). When the volume ratio is $>1:10$, the PLA did not result in much PL shift as a result of quick solidification of the PLA. Thus, the optimal volume ratio of PLA solution to parent $CsPbBr_3$ NCs solution is 1 : 10.

Based on the above optimized conditions, we synthesized a series of $CsPbX_3$ NCs with PL emission ranging from green to near UV. The representative digital photograph in Fig. 5a shows the bright luminescence of the solution under irradiation with a UV lamp (365 nm excitation source), indicating the formation of fluorescent $CsPbX_3$ NCs. The typical PL spectra of the as-prepared $CsPbX_3$ NCs were also investigated, as shown in Fig. 5b. The PL emission peaks range from 514 to 420 nm at different periods of time after the PLA solution was injected.

This journal is © The Royal Society of Chemistry 2018

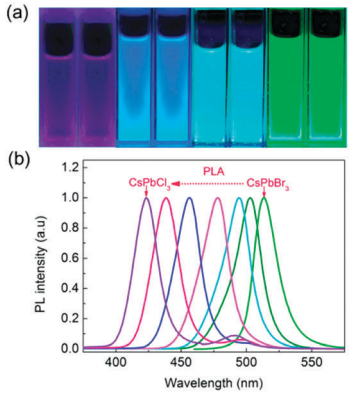

Fig. 5 (a) Representative digital photograph (365 nm excitation source) and (b) the PL spectra of anion-exchange synthesized $CsPbX_3$ NCs when PLA was added.

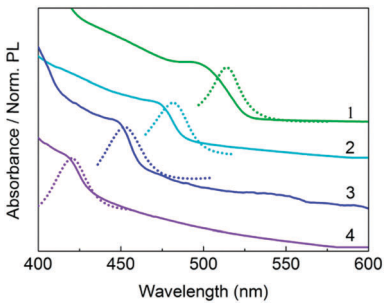

Fig. 6 UV-vis absorption (solid lines) and the corresponding PL spectra (dashed lines) of anion-exchanged samples from $CsPbBr_3$ to $CsPbCl_3$. The numbers 1, 2, 3, and 4 represent the anion-exchange reactions at different periods of time: 0 min, 30 min, 60 min, and 120 min, respectively.

Furthermore, we studied the representative UV-vis absorption and PL spectra of such exchanged $CsPbX_3$ NCs, as shown in Fig. 6. The parent $CsPbBr_3$ NC sample shows a strong absorption at approximately 490 nm and with a tail extending to the visible range. By adding PLA, the absorption peak gradually blue-shifted and reached to 415 nm finally. This shift consistent with the XRD result was a gradual shift due to the substitution of Cl^- with Br^- (Fig. 2). In addition, we observed that the absorption spectra gradually became broader as the PLA was added, which may be related to the interaction between PLA solution and $CsPbBr_3$ NCs. The PL spectra of the as-prepared $CsPbX_3$ NCs are Stokes-shifted with respect to the optical absorption. Using our method, the UV-vis absorption and PL spectra matched well with those of the directly synthesized $CsPbX_3$ NCs in previous reports,[9,25,29] indicating that the anion-exchange reaction was successful.

To observe the Br^- to Cl^- anion-exchange reactions *in situ*, the details of the typical transfer process are shown in Fig. 7a and b. At the beginning of the anion-exchange when the PLA was added, the PL intensity of $CsPbX_3$ NCs gradually decreased and the corresponding PL peak shifted slightly to blue (Fig. 7a). As the reaction proceeded, there was a more obvious blue-shift for the PL emission peak because of the Br^- partly replaced by Cl^- with the assistance of the PLA. Importantly, when the

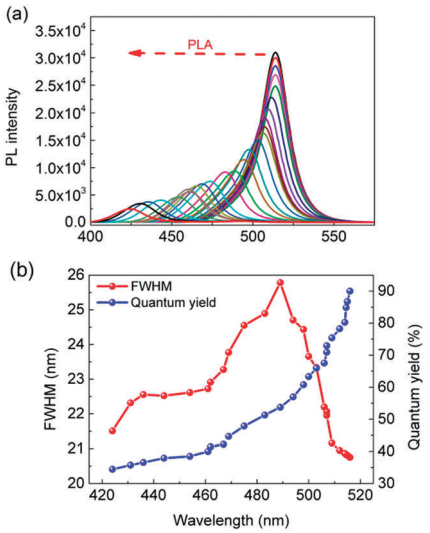

Fig. 7 (a) The details of the typical PL spectral shift process of $CsPbX_3$ NCs after PLA was added into $CsPbBr_3$ NCs. (b) The variation in the FWHM and QY of the selected samples corresponding to the typical PL spectral shift process of $CsPbX_3$ NCs.

anion-exchange was complete, the PL peak in the near UV region was unchanged and remained for several weeks in an ambient atmosphere. Beyond that, the variation in the full width at half maximum (FWHM) and the QY of the selected samples were investigated, as shown in Fig. 7b, where the FWHM first increases and then decreases while the QY shows a downward trend. The FWHM increased from 20.45 nm to 25.78 nm and then dropped to 21.62 nm, with the corresponding shift of the PL peak position being decreased from 514 nm to 484 nm and finally to 420 nm. The FWHM indicates that the as-prepared $CsPbX_3$ NCs have a narrow emission line width. Meanwhile, the QYs (33–90%) of the $CsPbX_3$ NCs gradually decreased along with the replacement of Br^- with Cl^-, which is consistent with a previous report.[24] The narrow emission line width and high QY of the $CsPbX_3$ NCs demonstrate their promising potential for optoelectronic applications.

Besides, we have evaluated the stability of the as-prepared $CsPbX_3$. The perovskite NCs synthesized *via* an inorganic anion-exchange method in the ambient environment exhibit poor stability, especially for $CsPbCl_3$ NCs. In order to determine the stability of $CsPbCl_3$ NCs, we compared our method with the conventional inorganic anion-exchange method. The details of the conventional anion-exchange method (namely direct synthesis) were described in the Experimental section. Compared with $CsPbCl_3$ NCs synthesized using the conventional anion-exchange method, the $CsPbCl_3$ NCs prepared by our method maintained a high PL QY in an ambient atmosphere at 4 °C for several weeks, as shown in Fig. 8. This result revealed that PLA not only promoted the Br^- to Cl^- anion-exchange but also improved the stability of NCs. Previous studies indicated that the stability of perovskite NCs is related to the surface ligand binding, which helps to prevent the NCs from aggregating.[31,45] However, during purification or storage, the surface ligands can detach from the perovskite NC surface,

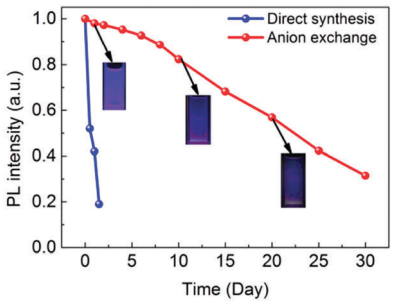

Fig. 8 The stability contrast of the $CsPbCl_3$ synthesized by the conventional inorganic anion-exchange method (direct synthesis) and the PLA-assistant anion-exchange method (anion-exchange) in the ambient environment. (Inset: Digital images of the corresponding $CsPbCl_3$ NCs under irradiation with a UV-vis lamp, λ = 365 nm).

leading to NC aggregation and decreased fluorescence. PLA can enhance the binding between the surface ligands and NCs, thereby increasing the stability of the NCs and reducing degradation.

3.3 The mechanism of interaction between PLA and $CsPbX_3$ NCs

To better understand the role of PLA on the PL spectral blue-shift, we designed and conducted four groups of experiments. G1, G2, G3, and G4 represent the $CsPbBr_3$ NC solution having nothing, chloroform, chloroform with PLA, and 1,4-dioxane with PLA added, respectively. These experiments were conducted under irradiation with a UV lamp (365 nm excitation source). The PL spectral shift at different periods of time was obtained, as shown in Fig. 9a–c. In the beginning, as shown in Fig. 9a, the PL intensities of all the samples decreased, but G3 has a more noticeable change in the PL intensity. As time goes on, the difference among them became larger, as shown in Fig. 9b and c. At 90 minutes (Fig. 9c), the G3 sample has a significant blue-shift and retains relatively high PL intensity,

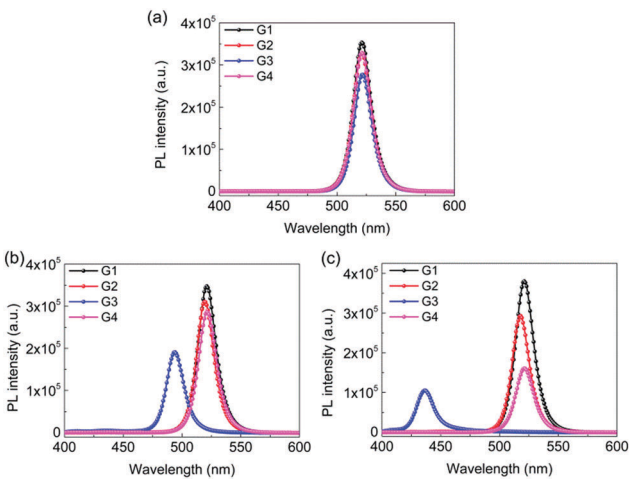

Fig. 9 The effect of four groups of experiments on the $CsPbBr_3$ PL spectral shift at different periods of time: (a) 0 min, (b) 30 min, and (c) 90 min. G1, G2, G3, and G4 represent the $CsPbBr_3$ NC solution having nothing, chloroform, chloroform with PLA, and 1,4-dioxane added, respectively.

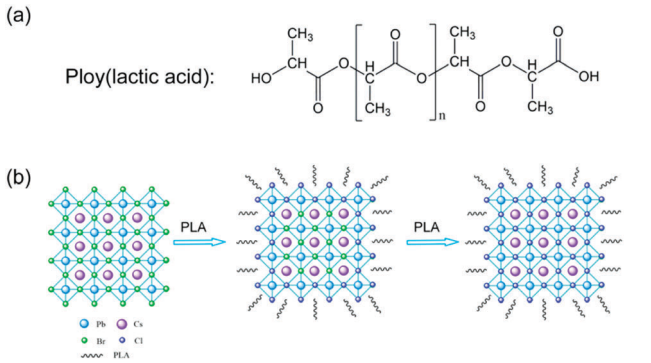

Fig. 10 (a) The molecular structure of PLA. (b) Schematic diagram of the Br^- to Cl^- anion-exchange at different periods of time when PLA was added. The substitution reaction between $CsPbBr_3$ NCs (with Br^-) and chloroform (with Cl^-) was occurred *via* PLA induced, and the stability $CsPbX_3$ NCs was improved by the dehydration condensation of PLA.

while the other three samples do not show a blue-shift. In addition, the G4 sample easily precipitated and thus resulted in fluorescence decay. Besides, we tried to directly add PLA into the $CsPbBr_3$ parent solution, but PLA cannot dissolve in toluene, thus it has no effect on the PL spectral shift. Based on this case, it is concluded that the Cl^- of the anion-exchange come from chloroform. Consequently, these results indicate that PLA promoted the Br^- to Cl^- anion-exchange between the chloroform and $CsPbBr_3$ NCs.

To explain the mechanism of interaction between PLA and $CsPbX_3$ NCs, a schematic diagram of the Br^- to Cl^- anion-exchange is shown in Fig. 10a and b. It is well known that the carboxyl and hydroxyl groups of compounds (such as oleic acid and benzyl alcohol) can interact with the surface of perovskite. In the case of PLA, there are two kinds of functional groups (–COOH: carboxyl, and –OH: hydroxyl) that can affect perovskite crystallization, as shown in Fig. 10a. Previous studies have shown that the bonding between Pb^{2+} and COO^- is more favorable to form than that between Pb^{2+} and –OH.[46–48] Therefore, when PLA was added to the $CsPbBr_3$ NCs solution, the carboxyl groups of PLA first attach to the surface of perovskite and bond with Pb^{2+} while the –OH and H^+ (from –COOH decomposition) were at the free state temporarily, as shown in Fig. 10b. Most polar alkyl halides are known to undergo concerted reductive dissociation into the halide ion (X^-) under external excitation (such as light, pressure, and solvent), which is also true for chloroform.[49,50] In addition, the bond energies of C–H (414.2 kJ mol^{-1}) and H–Cl (431 kJ mol^{-1}) are larger than that of C–Cl (339 kJ mol^{-1}), suggesting that chloroform can easily react with H^+ in solution, resulting in C–Cl bond breaking and free Cl^-. Moreover, the hydroxyl groups of PLA can modify the surface states of the $CsPbX_3$ NCs *via* hydrogen bonding with amino groups ($-NH_2$) and thus reduce the local concentrations of $-NH_2$.[51–53] Hence, the Cl^- can be easily absorb onto the surface of the $CsPbBr_3$ NCs. Therefore, it is possible that the substitution reaction between Br^- (from $CsPbBr_3$) and Cl^- (from chloroform) can be achieved *via* PLA introduction. Besides, when a larger amount of PLA was added, dehydration condensation occurred

 This journal is © The Royal Society of Chemistry 2018

between carboxyl and hydroxyl groups, forming a coating layer on the surface of the perovskite, which can improve $CsPbX_3$ NC stability. As a result, the combined action of carboxyl and hydroxyl groups of PLA led to the Br^- to Cl^- anion exchange and also improved the stability of $CsPbX_3$ NCs.

3.4 Evaluation of wLEDs with $CsPbX_3$ NC film performance

$CsPbX_3$ NCs are a promising candidate for applications in LEDs and displays because of their outstanding properties, including high PL QY and narrow emission bandwidth. We evaluated our synthesized $CsPbX_3$ NCs for white LED (wLED) applications, with the results shown in Fig. 11a–e. The wLEDs were fabricated by placing the green $CsPbBr_3$ NCs film and the red phosphor film above a blue LED chip, as shown in the inset of Fig. 11a. The EL spectra of Fig. 11a revealed that the $CsPbBr_3$ NCs have a narrow EL line width, which coincides with the white light requirement of backlight displays. The EL spectra of the wLEDs at different driving currents are shown in Fig. 11b. The spectral intensity increased with the increase of current from 20 to 350 mA and the spectral shape remained almost unchanged, indicating that the $CsPbBr_3$ NCs were not saturated by the blue light. The luminous efficiency and flux of the wLEDs were determined, as shown in Fig. 11c. The highest luminous efficiency was 62.93 lm W^{-1}, which is much higher than most previously reported values.[54–56] The CIE chromaticity coordinates in Fig. 11d show that the device presents warm white light (CCT is at about 4000 and (x, y) is at around (0.38, 0.37), respectively) at different currents. With increasing current, the CCT value shifts to a warm white color in accordance with the Planckian locus line. This result indicates that the device could be useful as a next-generation candidate for lamps and displays. Meanwhile, the performance of the wLEDs under different working conditions was investigated, as shown in Fig. 11e. After the wLEDs were in operation for 1 h, no evident change in the PL spectrum was observed, demonstrating good stability. Five hours later, the intensity of the green band slightly decreased while the blue and red bands were essentially unchanged. When the operation time was prolonged to 50 h, the EL spectral intensity of the wLEDs degraded 20%. These results indicate that the $CsPbBr_3$ NCs could serve as alternative candidates for the fabrication of high performance wLEDs.

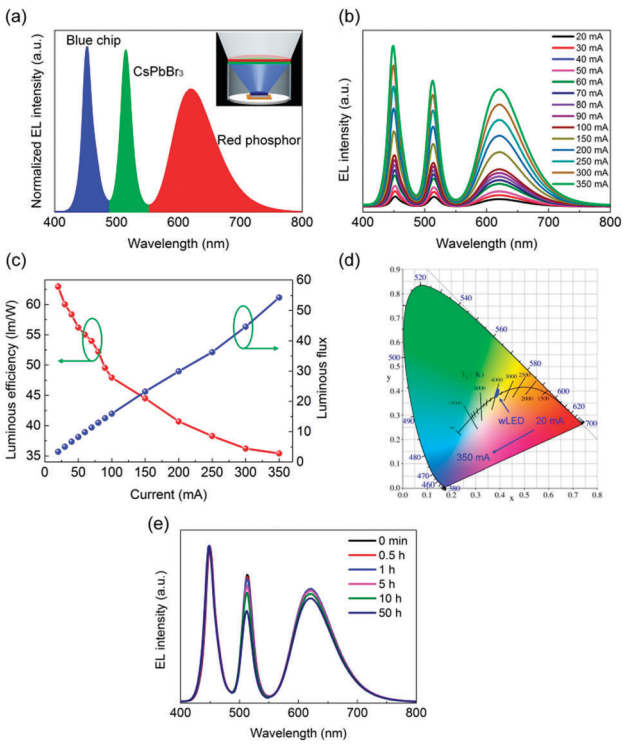

Fig. 11 (a) EL spectra of the wLED devices (inset: the schematic diagram of the device). (b) The EL spectra of the wLEDs operated with different forward-bias currents. (c) Luminous efficiency and luminous flux of the wLEDs. (d) The corresponding color coordinates of the wLEDs in a CIE diagram at different forward currents. The CCT is at about 4000 and (x, y) is at around (0.38, 0.37), respectively. (e) The EL spectra of the wLEDs measured at different working times (0–50 h).

4. Conclusion

In summary, we have demonstrated an anion-exchange reaction method assisted by organic molecules for synthesizing $CsPbX_3$ NCs with tunable optical properties. Using PLA in conjunction with a microreactor, the preparation of parent $CsPbBr_3$ NCs and the anion-exchange reaction can be completed in one-step, which is much more efficient than most previously reported methods. The XRD, TEM, and EDX results confirmed that Br^- was successfully replaced by Cl^- and the crystal structure of as-prepared $CsPbX_3$ remained the same. By varying key synthetic parameters (the mass fractions of PLA and the volume ratio of PLA solution to parent $CsPbBr_3$ NC solution), the PL spectra of $CsPbX_3$ NCs can be tuned from 514 nm to 420 nm while maintaining high PL QYs of 33–90%. The mechanism of the interaction between PLA and $CsPbBr_3$ NCs was investigated, and the results suggested that the combined action of the carboxyl and hydroxyl groups of the PLA promote the Br^- to Cl^- anion-exchange and improved the stability of $CsPbX_3$ NCs. Furthermore, the $CsPbBr_3$ NCs were used with a red phosphor on a blue LED chip, and a luminous efficacy of 62.93 lm W^{-1} under a 20 mA driving current was achieved with white light emission. The high-efficiency wLEDs demonstrate the strong potential of halide perovskite NCs for low-cost displays, lighting, and optical communication applications.

Conflicts of interest

There are no conflicts to declare.

Acknowledgements

We would like to thank the National Natural Science Foundation of China (51405161 and U1401249), the Science and Technology Program of Guangdong Province (2014B010-0121002, 2015B010132002, and 2015B010114003) for their financial support.

Notes and references

1 V. D'Innocenzo, G. Grancini, M. J. Alcocer, A. R. Kandada, S. D. Stranks, M. M. Lee, G. Lanzani, H. J. Snaith and A. Petrozza, *Nat. Commun.*, 2014, **5**, 3586.
2 C. Wehrenfennig, G. E. Eperon, M. B. Johnston, H. J. Snaith and L. M. Herz, *Adv. Mater.*, 2014, **26**, 1584–1589.
3 S. Stranks, G. Eperon, G. Grancini, C. Menelaou, M. Alcocer, T. Leijtens, L. Herz, A. Petrozza and H. J. Snaith, *Science*, 2013, **342**, 341–344.
4 G. Xing, N. Mathews, S. Sun, S. S. Lim, Y. M. Lam, M. Grätzel, S. Mhaisalkar and T. C. Sum, *Science*, 2013, **342**, 344.
5 Z. Chen, C. Zhang, X. F. Jiang, M. Liu, R. Xia, T. Shi, D. Chen, Q. Xue, Y. J. Zhao, S. Su, H. L. Yip and Y. Cao, *Adv. Mater.*, 2017, 29.
6 L. Protesescu, S. Yakunin, M. I. Bodnarchuk, F. Krieg, R. Caputo, C. H. Hendon, R. X. Yang, A. Walsh and M. V. Kovalenko, *Nano Lett.*, 2015, **15**, 3692.
7 X. Li, F. Cao, D. Yu, J. Chen, Z. Sun, Y. Shen, Y. Zhu, L. Wang, Y. Wei and Y. Wu, *Small*, 2017, **13**, 1603996.
8 E. Yassitepe, Z. Yang, O. Voznyy, Y. Kim, G. Walters, J. A. Castañeda, P. Kanjanaboos, M. Yuan, X. Gong and F. Fan, *Adv. Funct. Mater.*, 2016, 26.
9 P. Ramasamy, D.-H. Lim, B. Kim, S.-H. Lee, M.-S. Lee and J.-S. Lee, *Chem. Commun.*, 2016, **52**, 2067–2070.
10 D. Amgar, S. Aharon and L. Etgar, *Adv. Funct. Mater.*, 2016, **26**, 8576–8593.
11 J. Song, J. Li, X. Li, L. Xu, Y. Dong and H. Zeng, *Adv. Mater.*, 2015, **27**, 7162.
12 A. Swarnkar, R. Chulliyil, V. K. Ravi, M. Irfanullah, A. Chowdhury and A. Nag, *Angew. Chem., Int. Ed.*, 2015, **54**, 15424.
13 Y. H. Song, J. S. Yoo, B. K. Kang, S. H. Choi, E. K. Ji, H. S. Jung and D. H. Yoon, *Nanoscale*, 2016, **8**, 19523.
14 A. Swarnkar, A. R. Marshall, E. M. Sanehira, B. D. Chernomordik, D. T. Moore, J. A. Christians, T. Chakrabarti and J. M. Luther, *Science*, 2016, **354**, 92–95.
15 F. Hetsch, N. Zhao, S. V. Kershaw and A. L. Rogach, *Mater. Today*, 2017, **16**, 312–325.
16 S. A. Veldhuis, P. P. Boix, N. Yantara, M. Li, T. C. Sum, N. Mathews and S. G. Mhaisalkar, *Adv. Mater.*, 2016, **28**, 6804.
17 X. Li, D. Yu, F. Cao, Y. Gu, Y. Wei, Y. Wu, J. Song and H. Zeng, *Adv. Funct. Mater.*, 2016, **26**, 5903–5912.
18 M. Meyns, M. Peralvarez, A. Heuer-Jungemann, W. Hertog, M. Ibanez, R. Nafria, A. Genc, J. Arbiol, M. V. Kovalenko, J. Carreras, A. Cabot and A. G. Kanaras, *ACS Appl. Mater. Interfaces*, 2016, **8**, 19579–19586.
19 I. Dursun, C. Shen, M. R. Parida, J. Pan, S. P. Sarmah, D. Priante, N. Alyami, J. Liu, M. I. Saidaminov, M. S. Alias, A. L. Abdelhady, T. K. Ng, O. F. Mohammed, B. S. Ooi and O. M. Bakr, *ACS Photonics*, 2016, **3**, 1150–1156.
20 P. K. Jain, L. Amirav, S. Aloni and A. P. Alivisatos, *J. Am. Chem. Soc.*, 2010, **132**, 9997–9999.
21 R. D. Robinson, B. Sadtler, D. O. Demchenko, C. K. Erdonmez, L. W. Wang and A. P. Alivisatos, *Science*, 2007, **317**, 355–358.
22 H. Li, R. Brescia, M. Povia, M. Prato, G. Bertoni, L. Manna and I. Moreels, *J. Am. Chem. Soc.*, 2013, **135**, 12270–12278.
23 B. A. Koscher, N. D. Bronstein, J. H. Olshansky, Y. Bekenstein and A. P. Alivisatos, *J. Am. Chem. Soc.*, 2016, 138.
24 G. Nedelcu, L. Protesescu, S. Yakunin, M. I. Bodnarchuk, M. J. Grotevent and M. V. Kovalenko, *Nano Lett.*, 2015, **15**, 5635–5640.
25 D. Zhang, Y. Yang, Y. Bekenstein, Y. Yu, N. A. Gibson, A. B. Wong, S. W. Eaton, N. Kornienko, Q. Kong, M. Lai, A. P. Alivisatos, S. R. Leone and P. Yang, *J. Am. Chem. Soc.*, 2016, **138**, 7236–7239.
26 V. K. Ravi, G. B. Markad and A. Nag, *ACS Energy Lett.*, 2016, 1.
27 I. Karimata, Y. Kobori and T. Tachikawa, *J. Phys. Chem. Lett.*, 2017, **8**, 1724–1728.
28 M. Li, X. Zhang, S. Lu and P. Yang, *RSC Adv.*, 2016, **6**, 103382–103389.
29 D. M. Jang, K. Park, D. H. Kim, J. Park, F. Shojaei, H. S. Kang, J. P. Ahn, J. W. Lee and J. K. Song, *Nano Lett.*, 2015, **15**, 5191.
30 Q. A. Akkerman, V. D'Innocenzo, S. Accornero, A. Scarpellini, A. Petrozza, M. Prato and L. Manna, *J. Am. Chem. Soc.*, 2015, **137**, 10276–10281.
31 T. Zhang, G. Li, Y. Chang, X. Wang, B. Zhang, H. Mou and Y. Jiang, *CrystEngComm*, 2016, 1137–1240.
32 D. Parobek, Y. Dong, T. Qiao, D. Rossi and D. H. Son, *J. Am. Chem. Soc.*, 2017, **139**, 4358–4361.
33 Y. Zhang, C. F. Wang, L. Chen, S. Chen and A. J. Ryan, *Adv. Funct. Mater.*, 2016, **25**, 7396.
34 A. M. Nightingale and J. C. D. Mello, *J. Mater. Chem.*, 2010, **20**, 8454–8463.
35 C. Wiles and P. Watts, *Chem. Commun.*, 2011, **47**, 6512–6535.
36 P. W. Dunne, C. L. Starkey, M. Gimenofabra and E. H. Lester, *Nanoscale*, 2014, **6**, 2406–2418.
37 I. Lignos, S. Stavrakis, G. Nedelcu, L. Protesescu, A. J. deMello and M. V. Kovalenko, *Nano Lett.*, 2016, **16**, 1869–1877.
38 R. W. Epps, K. C. Felton, C. W. Coley and M. Abolhasani, *Lab Chip*, 2017, **17**, 4040–4047.
39 K. Ma, X.-Y. Du, Y.-W. Zhang and S. Chen, *J. Mater. Chem. C*, 2017, **5**, 9398–9404.
40 L. Protesescu, S. Yakunin, M. I. Bodnarchuk, F. Krieg, R. Caputo, C. H. Hendon, R. X. Yang, A. Walsh and M. V. Kovalenko, *Nano Lett.*, 2015, **15**, 3692.
41 Z. Wang, B. Fu, S. Zou, B. Duan, C. Chang and B. Yang, *Nano Res.*, 2016, **9**, 214–223.
42 A. M. Brouwer, *Pure Appl. Chem.*, 2011, **83**, 2213–2228.
43 K. H. Wang, L. Wu, L. Li, H. B. Yao, H. S. Qian and S. H. Yu, *Angew. Chem.*, 2016, **55**, 8328.
44 P. Cottingham and R. L. Brutchey, *Chem. Commun.*, 2016, **52**, 5246.
45 R. J. De, M. Ibáñez, P. Geiregat, G. Nedelcu, W. Walravens, J. Maes, J. C. Martins, D. I. Van, M. V. Kovalenko and Z. Hens, *ACS Nano*, 2016, **10**, 2071.
46 S. Ananthakumar, J. R. Kumar and S. M. Babu, *J. Photonics Energy*, 2016, **6**, 042001.
47 X. He, Y. Qiu and S. Yang, *Adv. Mater.*, 2017, 29.
48 S. A. Veldhuis, K. E. T. Yong, A. Bruno, S. S. H. Dintakurti, S. Bhaumik, S. Muduli, M. Li, N. Mathews, T. C. Sum and S. G. Mhaisalkar, *Nano Lett.*, 2017, 7424–7432.

This journal is © The Royal Society of Chemistry 2018

49 J. M. Saveant, *J. Am. Chem. Soc.*, 1992, **114**, 10595–10602.
50 A. A. Isse, A. Gennaro, C. Y. Lin, J. L. Hodgson, M. L. Coote and T. Guliashvili, *J. Am. Chem. Soc.*, 2011, **133**, 6254–6264.
51 T. Chiba, K. Hoshi, Y. J. Pu, Y. Takeda, Y. Hayashi, S. Ohisa, S. Kawata and J. Kido, *ACS Appl. Mater. Interfaces*, 2017, **9**, 18054–18060.
52 F. Fang, W. Chen, Y. Li, H. Liu, M. Mei, R. Zhang, J. Hao, M. Mikita, W. Cao, R. Pan, K. Wang and X. W. Sun, *Adv. Funct. Mater.*, 2018, **28**, 1706000.
53 Q. Jing, M. Zhang, X. Huang, X. Ren, P. Wang and Z. Lu, *Nanoscale*, 2017, **9**, 7391–7396.
54 D. Chen, G. Fang and X. Chen, *ACS Appl. Mater. Inter.*, 2017, **9**, 40477–40487.
55 J.-Y. Sun, F. T. Rabouw, X.-F. Yang, X.-Y. Huang, X.-P. Jing, S. Ye and Q.-Y. Zhang, *Adv. Funct. Mater.*, 2017, **27**, 1704371.
56 G. Yang, Q. Fan, B. Chen, Q. Zhou and H. Zhong, *J. Mater. Chem. C*, 2016, **4**, 11387–11391.

This journal is © The Royal Society of Chemistry 2018